

SOAR observations of the high-viscosity accretion disc of the dwarf nova V4140 Sagittarii in quiescence and in outburst ^{*}

Raymundo Baptista^{1†}, Bernardo W. Borges² & Alexandre S. Oliveira³

¹*Departamento de Física, Universidade Federal de Santa Catarina, Trindade, 88040-900, Florianópolis, SC, Brazil*

²*Universidade Federal de Santa Catarina, Campus Araranguá, CEP 88905-120, Araranguá, SC, Brazil*

³*IP&D, Universidade do Vale do Paraíba, CEP 12244-000, São José dos Campos, SP, Brazil*

Accepted 2016 September 5. Received 2016 September 5; in original form 2016 January 26

ABSTRACT

We report the analysis of 22 B-band light curves of the dwarf nova V4140 Sgr obtained with SOI/SOAR during two nights along the decline of a superoutburst in 2006 Sep 12-24 and in quiescence over 50 days following the superoutburst. Three-dimensional eclipse mapping of the outburst light curves indicates that the accretion disc is elliptical (eccentricity $e = 0.13$) and that superhump maximum occurs when the mass donor star is aligned with the bulge of the elliptical disc. The accretion disc is geometrically thin both in outburst and in quiescence; it fills the primary Roche lobe in outburst and shrinks to about half this size in quiescence. The stability of the eclipse shape, width and depth along quiescence and the derived disc surface brightness distribution indicate that the quiescent accretion disc is in a high-viscosity, steady-state. Flickering mapping of the quiescent data reveal that the low-frequency flickering arises from an azimuthally-extended stream-disc impact region at disc rim and from the innermost disc region, whereas the high-frequency flickering originates in the accretion disc. Assuming the disc-related flickering to be caused by fluctuations in the energy dissipation rate induced by magneto-hydrodynamic turbulence (Geertsema & Achterberg 1992), we find that the quiescent disc viscosity parameter is large $\alpha \simeq 0.2 - 0.4$ at all radii. The high-viscosity quiescent disc and the inferred low disc temperatures in superoutburst are inconsistent with expectations of the disc-instability model, and lead to the conclusion that the outbursts of V4140 Sgr are powered by mass transfer bursts from its donor star.

Key words: accretion, accretion discs – binaries: eclipsing – novae, cataclysmic variables – stars: dwarf novae – stars: individual (V4140 Sagittarii)

1 INTRODUCTION

In dwarf novae, mass is transferred from a late-type star (the secondary) to a companion white dwarf (WD) via an accretion disc. They show recurrent outbursts on timescales of days-months, in which the disc brightens by factors 20-100 for $\simeq 1 - 10$ days. Outbursts are explained in terms of

either a thermal-viscous disc-instability model (DIM, e.g., Cannizzo 1993; Lasota 2001) or a mass-transfer instability model (MTIM, e.g., Bath 1975). DIM predicts matter accumulates in a low viscosity ¹ disc during quiescence ($\alpha_{\text{quies}} \sim 10^{-2}$) which switches to a high-viscosity regime during outbursts, whereas in MTIM the disc viscosity is always the same ($\alpha \sim 0.1 - 1$, from the decline timescale of outbursting dwarf novae, e.g., Warner 1995). Therefore, es-

^{*} Based on observations obtained at the Southern Astrophysical Research (SOAR) telescope, which is a joint project of the Ministério da Ciência, Tecnologia, e Inovação (MCTI) da República Federativa do Brasil, the U.S. National Optical Astronomy Observatory (NOAO), the University of North Carolina at Chapel Hill (UNC), and Michigan State University (MSU).

[†] E-mail: raybap@gmail.com

¹ here we adopt the prescription of Shakura & Sunyaev (1973) for the accretion disc viscosity, $\nu = \alpha c_s H$, where α is the non-dimensional viscosity parameter, c_s is the local sound speed and H is the disc scaleheight.

timating α of a quiescent disc is key to gauge which model is at work in a given dwarf nova.

Aside of the normal outbursts, the short-period dwarf novae of the SU UMa type show longer, slightly brighter and more regular superoutbursts, during which a hump-shaped brightness modulation (named *superhump*) with period slightly longer than the orbital period P_{orb} is seen in their light curves (Warner 1995; Hellier 2001). The most promising explanation for superhumps is given by the tidal resonance instability model (Whitehurst 1988; Hirose & Osaki 1990; Lubow 1994): during a superoutburst, the accretion disc expands beyond the 3:1 resonance radius, R_{31} , and a tidal instability sets in, giving rise to an elliptical, slowly precessing disc. Superhump modulation then arises from the periodic tidal interaction between the outer elliptical disc and the mass-donor star (normal superhumps) or by the varying release of gravitational energy at the point where the gas stream hits the precessing elliptical disc outer edge (late superhumps), at the beat period between the orbital and the disc precession period, $1/P_{\text{sh}} = 1/P_{\text{orb}} - 1/P_{\text{prec}}$. Eclipse mapping (Horne 1985) is a powerful tool to test for the presence of elliptical discs in outbursting dwarf novae as well as to check whether the orientation of the ellipse is according to the expectation of the tidal instability model (e.g., O’Donoghue 1990; Rolfe et al. 2000).

Flickering is the intrinsic brightness fluctuation of 0.01–1 mag on timescales of seconds to dozens of minutes seen in dwarf novae light curves. Optical studies (e.g., Bruch 1992, 1996, 2000; Baptista & Bortoletto 2004) suggest there may be three different sources of flickering in dwarf novae and novalike systems, the relative importance of which varies from system to system: (i) the stream-disc impact region (possibly because of unsteady mass transfer or post-shock turbulence, Warner & Nather 1971; Shu 1976), (ii) the innermost disc regions around the WD (possibly powered by unsteady WD accretion or post-shock turbulence in the boundary layer between disc and WD, Elsworth & James 1982; Bruch 1992), and (iii) the accretion disc itself (probably as a consequence of magneto-hydrodynamic (MHD) turbulence or events of magnetic reconnection at the disc atmosphere, Geertsema & Achterberg 1992; Kawaguchi et al. 2000; Baptista & Bortoletto 2004). The power density spectrum (PDS) of the flickering is characterized by a continuum power-law, $P(f) \propto f^{-n}$, with $n \simeq 1-3$ (Bruch 1992), which flattens below a given cut-off frequency f_c .

Currently, the most promising explanation for the anomalously large viscosity of accretion discs is related to MHD turbulence in the differentially rotating disc gas (driven by the magnetorotational instability, MRI, see Balbus & Hawley 1991; Hawley & Balbus 1991). Most of the studies on this subject over the last two decades focused on confirming that MRI leads to self-sustained, turbulent and efficient outward flow of angular momentum and inward flow of disc matter (e.g., Balbus & Hawley 1998; Beckwith et al. 2011, and references therein), and on the comparison of the numerically derived values of α with those inferred by the decline timescale of outbursting dwarf novae (e.g., King et al. 2007; Hirose et al. 2014). On the other hand, the study of Geertsema & Achterberg (1992) focused on the time variability of the viscous energy release in a MHD turbulent disc. They found that MHD turbulence leads to large fluctuations in the energy dissipation rate per unit area at the

disc surface, $D(R)$, which they suggested could be a source of flickering in mass-exchanging binaries. Indeed, the PDS of the fluctuations in their study resemble those of flickering sources, with a power-law dependency of similar index range and a flat slope at low-frequencies. The interpretation of the fluctuations in $D(R)$ as the stochastic and statistically independent release of energy from a large number of turbulent eddies leads to a direct relation between the relative amplitude of the energy fluctuations $\sigma_D/\langle D \rangle$ and the disc viscosity parameter, $\sigma_D/\langle D \rangle \propto \alpha^{1/2} (H/R)^{1/2}$, providing an interesting observational way to estimate the local accretion disc viscosity parameter (see, e.g., Baptista & Bortoletto 2004). For a thin accretion disc ($H \simeq 0.01 R$), the above relation predicts that low-viscosity discs ($\alpha \sim 10^{-2}$) should show low-amplitude disc flickering (hardly detectable at a level ≤ 1 per cent), whereas high-viscosity discs ($\alpha = 0.1-1$) should display detectable flickering with relative amplitudes in the range 2.5–7.5 per cent. There is observational support for this prediction: e.g., the accretion disc seems the dominant source of flickering in the high-viscosity discs of the nova-like systems RW Tri (Horne & Stiening 1985) and UX UMa (Bruch 2000), whereas there is no evidence of disc-related flickering in the low-viscosity accretion discs of the dwarf novae U Gem (Warner & Nather 1971) and IP Peg (Bruch 2000) in quiescence.

V4140 Sgr is an 88-min period eclipsing SU UMa type dwarf nova (Jablonski & Steiner 1987; Baptista et al. 1989) showing low-amplitude (~ 1 mag), 5–10 d long outbursts recurring every 80–90 d and longer, brighter superoutbursts where superhumps appear in its light curve (Borges & Baptista 2005). Here we report the analysis of a sample of light curves of V4140 Sgr with eclipse mapping techniques to trace the evolution of the surface brightness of its accretion disc during decline from a superoutburst, to locate the sources of flickering in the binary and to estimate the radial run of the quiescent disc viscosity parameter. Section 2 reports the observations and data reduction procedures. Data analysis and results are presented in section 3, discussed in section 4, and summarized in section 5.

2 OBSERVATIONS AND DATA REDUCTION

Time series of B-band CCD photometry of V4140 Sgr were obtained along 2006 with the SOAR Optical Imager (SOI) at the 4.1 m SOAR telescope, in Cerro Pachón, Chile. The SOI camera has a mini-mosaic of two back illuminated E2V 2048 \times 4096 pixels CCDs covering a 5.26 arcminute square field of view. The SOI detectors are mounted with their long sides parallel and spaced 102 pixels apart, resulting in a 8'' gap between the individual CCD images. All observations were performed in its 4 \times 4 pixels binning and fast-readout mode (6.1 s total readout time) at a spatial scale of 0.31'' pixel $^{-1}$. The observations are summarized in Table 1. Column 3 lists the number of points in the light curve (N_p), column 4 gives the exposure time in seconds (Δt). Column 5 lists the eclipse cycle number (E); observations that do not cover the eclipse are indicated in parenthesis, and those with incomplete eclipse phase coverage are indicated by a colon after the cycle. Column 7 gives an estimate of the quality of each run. The observations comprise 22 light curves ob-

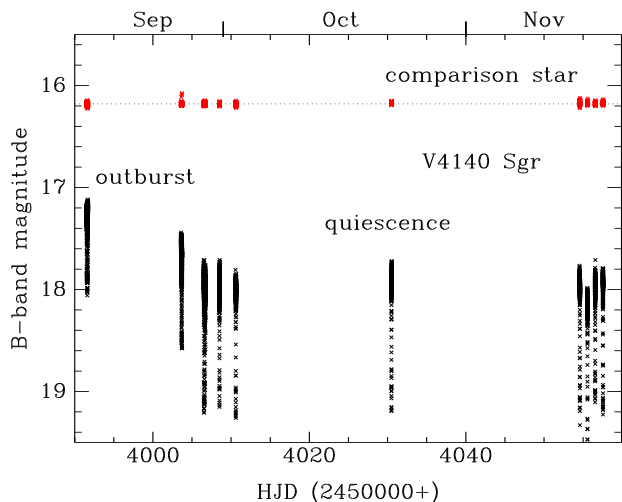


Figure 1. Combined SOAR light curves of V4140 Sgr (black crosses) for the epoch 2006 September to November. Excursions to higher magnitudes indicate eclipses. Measurements of a brighter comparison star are shown in red for illustrations purposes.

tained with the same instrument and telescope, ensuring a high degree of uniformity to the data set.

Data reduction procedures included bias subtraction, flat-field correction, cosmic rays removal and aperture photometry extraction. Time series were constructed by computing the magnitude difference between the variable and a bright reference comparison star $60''$ S of the variable (star C1 in the finding chart of [Borges & Baptista 2005](#)) with scripts based on the aperture photometry routines of the `apphot/IRAF` package². Light curves of other comparison stars in the field were also computed in order to check the quality of the night and the internal consistency and stability of the photometry over the time span of the observations. The magnitude and colors of the reference star were tied to the Johnsons-Cousins BVRI system ([Bessell 1990](#)) from observations of this star and of standard stars ([Graham 1982](#); [Stone & Baldwin 1983](#)) made on a photometric night. The reference star has a calibrated magnitude of $B = 14.75 \pm 0.05$ mag. We used the relations of [Lamla \(1981\)](#) to transform its B -band magnitude to flux units and to convert the light curves of the variable star from magnitude difference to absolute flux with an estimated photometric accuracy of 5 per cent. Moreover, the analysis of the light curves of field comparison stars of brightness comparable to that of the variable indicates that the internal error of the photometry is less than 2 per cent. The error in the photometry of the variable is derived from the photon count noise and is transformed to flux units using the same relation applied to the data. The individual light curves have typical signal-to-noise ratios of $S/N = 50$ out-of-eclipse and $S/N = 10$ -20 at mid-eclipse.

Fig. 1 shows the 2006 observations of V4140 Sgr. It was caught in outburst in Sep 12 ($\simeq 1$ mag brighter than in quies-

cence), while the Sep 24 observations frame the decline from that outburst. The object was back to its quiescent state from Sep 27 onwards. Given the typical shape and length of the V4140 Sgr outbursts ([Borges & Baptista 2005](#)), the Sep 12 data probably correspond to the outburst plateau phase (i.e., past outburst maximum). As previously noted by [Borges & Baptista \(2005\)](#), the eclipses in outburst are shallower than in quiescence, indicating that the brightness increase is mainly from the outer and partially eclipsed disc regions. The presence of superhumps in the outburst light curves (Sect. 3.2) indicates that this was a superoutburst.

3 DATA ANALYSIS AND RESULTS

3.1 The Light Curves

The light curves were phase-folded according to the linear plus sinusoidal ephemeris of [Baptista et al \(2003\)](#),

$$T_{mid} = \text{BJDD } 2\,446\,261.671\,50 + 0.061\,429\,6757 \times E + 19 \times 10^{-5} \cos \left[2\pi \left(\frac{E - 3 \times 10^3}{41 \times 10^3} \right) \right] d. \quad (1)$$

where E is the cycle number and T_{mid} gives the WD mid-eclipse times. We checked whether this ephemeris correctly centred the WD eclipse by median combining all quiescent data, computing the derivative of the combined light curve, and measuring the phases of minimum/maximum in the derivative on the assumption that they indicate the mid-ingress/egress phases of the WD eclipse. This leads to a WD eclipse width of $\Delta\phi = 0.0384 \pm 0.0006$ cycle, in good agreement with the value derived by [Baptista et al. \(1989\)](#). We also find a WD mid-eclipse phase of $\phi_0 = +0.0039$ cycle, indicating that the observed eclipses occurred 20.5 s after the prediction of the ephemeris of Eq.(1). All light curves were then offset by -0.0039 cycle to make the WD eclipse centre coincident with phase zero.

Fig. 2 shows phase-folded light curves of V4140 Sgr grouped per brightness state. The median quiescent light curve displays a steep, narrow eclipse with a long egress shoulder and a weak orbital hump with an apparent maximum at phase -0.08 cycle, signaling a small contribution from the bright spot at disc rim to the total flux. The superoutburst light curves show strong flickering (at $\simeq 20$ per cent level) and a pronounced, broad superhump centred at phase zero. In the decline light curves, flickering amplitude is reduced (in absolute and relative terms) and the superhump maximum is displaced to phase $\simeq +0.25$ cycle. Flares and flickers occurring right before ingress and just after egress of the WD suggest that a significant fraction of the flickering in superoutburst and decline arises from the inner disc regions. Unfortunately, the small number of light curves covering superoutburst and decline prevents us from applying flickering mapping techniques (see Sect. 3.4) to derive the spatial distribution of the flickering sources at these brightness states. The total width of the eclipses decreases with decreasing brightness suggesting that the accretion disc shrinks along the decline from superoutburst, being smallest in quiescence. Furthermore, the depth of the eclipses increases with decreasing brightness signaling that the relative

² IRAF is distributed by National Optical Astronomy Observatories, which is operated by the Association of Universities for Research in Astronomy, Inc., under contract with the National Science Foundation.

Table 1. Journal of the observations

Date (UT) (2006)	HJD start (2.450.000+)	N_p	Δt (s)	E ^a (cycle)	Phase Range	Night Quality ^b	Seeing (")
Sep 12	3991.53678	528	3.7	125833	-0.50, +0.50	A	0.8-2.0
"	3991.58268	446	3.7	125834	-0.50, +0.50	B	
"	3991.64405	467	3.7	125835	-0.50, +0.34	B	
Sep 24	4003.60079	205	3.7	(126029)	+0.14, +0.50	A	0.7-1.0
"	4003.62291	548	3.7	126030	-0.50, +0.50	B	
"	4003.68432	385	3.7	126031	-0.50, +0.20	B	
Sep 27	4006.50008	77	3.7	(126076)	+0.34, +0.50	C	0.7-0.9
"	4006.51006	547	3.7	126077	-0.50, +0.50	B	
"	4006.57151	557	3.7	126078	-0.50, +0.50	B	
"	4006.64293	548	3.7	126079	-0.50, +0.50	B	
"	4006.69433	270	3.7	126080:	-0.50, -0.02	B	
Sep 29	4008.49251	428	3.7	126109	-0.23, +0.76	A	0.7-0.9
Oct 01	4010.54703	95	5.0	(126142)	+0.29, +0.50	B	0.8-1.1
"	4010.56445	442	5.0	126143	-0.50, +0.50	B	
"	4010.62589	207	5.0	126144:	-0.50, -0.03	B	
Oct 21	4030.48861	359	4.0	126467	-0.16, +0.52	A	0.7-0.8
Nov 14	4054.52175	202	4.0	(126858)	+0.07, +0.50	A	0.8-1.0
"	4054.54806	499	4.0	126859	-0.50, +0.44	A	
Nov 15	4055.51412	131	4.0	(126874)	+0.23, +0.50	A	0.8-1.1
"	4055.53092	405	4.0	126875	-0.50, +0.26	A	
Nov 16	4056.51947	370	4.0	126891	-0.41, +0.29	A	0.9-1.2
Nov 17	4057.51611	359	4.0	126907	-0.18, +0.51	B	1.0-1.6

^a With respect to the ephemeris of eq. (1).

^b Sky conditions: (A) photometric, (B) good, (C) poor (large variations, clouds, or both).

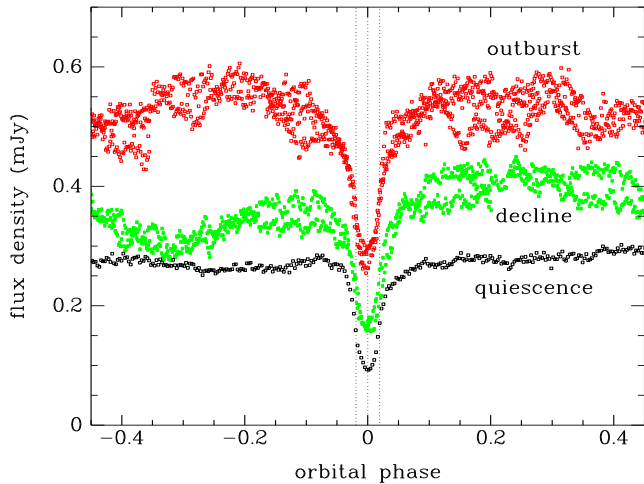


Figure 2. Phase-folded light curves of V4140 Sgr for Sep 12 (*outburst*, red open squares) and Sep 24 (*decline*, green filled squares), together with the median of the 16 individual light curves in quiescence (*quiescence*, black open squares). Vertical dotted lines mark mid-eclipse and WD ingress/egress phases.

contribution of the outer disc regions to the total flux decreases along the decline and is also smallest in quiescence.

3.2 On the Nature of the Outburst

Was the 2006 Sep outburst a normal one or a superoutburst? A straightforward way to address this questions is by searching for superhumps in the outburst and decline light curves.

In order to detect non-orbital periodicities, we removed the eclipses (phase range -0.1 to $+0.1$) from the light curves and computed Lomb-Scargle periodograms (Press et al. 1992) separately for the Sep 12 and Sep 24 data. The power spectrum of the latter data set shows a periodicity at frequency $f_{sh} = 14.9 \pm 1.0 \text{ cycle d}^{-1}$, corresponding to a period of $P_{sh} = 0.067 \pm 0.005 \text{ d}$, where the quoted uncertainty is derived from the width at half power of the observed peak. The same periodicity is found in the Sep 12 periodgram, although the corresponding power spectrum peak is less pronounced in this case.

This period is consistently longer than the orbital period, and is the same in both nights within the uncertainties. Moreover, the maximum of the observed modulation coincides with phase zero on Sep 12 and has shifted to phase $\simeq +0.25$ cycle on Sep 24 (Fig.2), indicating that it is not the consequence of anisotropic emission from a bright spot at disc rim, and confirming that P_{sh} is different from the orbital period. Also, the length of the 2006 Sep outburst is at least 13 days (it probably started before Sep 12), which is clearly longer than the typical 5-10 d duration of the normal outbursts of this dwarf nova (Borges & Baptista 2005). These evidences give us confidence that the observed modulations in Sep 12 and Sep 24 light curves are indeed superhumps and, therefore, that these observations framed a superoutburst of V4140 Sgr.

As a consequence of the short time span of the observations (only 2-3 binary orbits in each date), the uncertainty in P_{sh} is too large to allow a meaningful derivation of a superhump period excess from P_{sh} . We attempted to increase the accuracy of the measurement of P_{sh} by computing a power spectrum of the combined light curve of both nights.

However, no periodicity other than harmonics of the orbital period appears in this case, suggesting a significant change in phase of the superhump signal along this time interval – as is usual in superoutbursting dwarf novae (e.g., Patterson et al. 2000).

3.3 3D Eclipse Mapping in Outburst

We grouped the data per outburst stage to generate phase-binned, median-averaged light curves for the ‘outburst’ (Sep 12 data), ‘decline’ (Sep 24 data) and ‘quiescence’ (the remaining data sets) brightness states. The resulting light curves have phase resolutions of 0.003 cycle during eclipse (phase range -0.1 to $+0.1$ cycle) and of 0.009 cycle outside of eclipse. Only orbital phases in the range -0.4 to $+0.4$ cycle are included because our eclipse mapping algorithm does not handle a possible eclipse of the secondary star by the accretion disc (at phase ± 0.5).

Three-dimensional (3D) maximum entropy eclipse mapping techniques were applied to these light curves in order to investigate the source of the superhump and to follow the evolution of the disc surface brightness distribution along the superoutburst decline. The reader is referred to Horne (1985) for the historical presentation, Rutten (1998) for a description and performance tests of the 3D eclipse mapping algorithm, and Baptista (2001) for a more recent review on eclipse mapping techniques.

Our 3D eclipse map consists of a grid of 51×51 pixels on a conical surface with side $2 R_{L1}$ (where R_{L1} is the distance from disc centre to the inner Lagrangian point) centred at the WD position and inclined at a half-opening angle β with respect to the orbital plane, plus a circular rim of 102 pixels orthogonal to the orbital plane at a distance R_d ($< R_{L1}$) from the disc centre. The disc rim allows us to model out-of-eclipse modulations (such as anisotropic emission from the bright spot at stream-disc impact) as the fore-shortening of an azimuthally-dependent brightness distribution in the disc rim pixels (Bobinger et al. 1997; Ribeiro et al. 2007). The eclipse geometry is defined by the mass ratio q and the inclination i , and the scale of the map is set by R_{L1} . We adopted $R_{L1} = (0.427 \pm 0.035) R_{\odot}$, $q = 0.125 \pm 0.015$ and $i = 80.2^{\circ} \pm 0.5^{\circ}$ (Borges & Baptista 2005), which correspond to a WD eclipse width of $\Delta\phi = 0.0378 \pm 0.0005$ cycle (Baptista et al. 1989). This combination of parameters ensures that the WD is at the centre of the map.

The light curves were analyzed by the 3D eclipse mapping algorithm to solve for a map of the disc + rim surface brightness distribution. The reconstructions were performed with a polar Gaussian default function (Rutten et al. 1992) with radial blur width $\Delta r = 0.02 R_{L1}$ and azimuthal blur width $\Delta\theta = 30^{\circ}$, and reached a final reduced chi-square $\chi_{\text{red}}^2 \simeq 1$ for all light curves. The uncertainties in the eclipse maps were derived from Monte Carlo simulations with the light curves using the bootstrap technique (Efron 1982; Watson & Dhillon 2001), generating a set of 20 randomized eclipse maps (see Rutten et al. 1992). These are combined to produce a map of the standard deviations with respect to the true map. A map of the statistical significance (or the inverse of the relative error) is obtained by dividing the true eclipse map by the map of the standard deviations (Baptista et al. 2005). The uncertainties obtained with this procedure are used to draw the contour maps of Fig. 3, and

to estimate the uncertainties in the derived disc rim intensity (Fig. 3) and radial brightness temperature distributions (Fig. 4).

3.3.1 Disc rim and disc half-opening angle

An entropy landscape technique was used to derive the best-fit disc rim radius R_d and half-opening angle β for each brightness state (see Appendix). We obtained reconstructions for disc rims in the range $(0.35 - 0.85) R_{L1}$ at steps of $0.05 R_{L1}$, and half-opening angles in the range $(0^{\circ} - 6^{\circ})$ at steps of 0.5° , and investigated the resulting space of parameters in search of the combination (R_d, β) that yields the eclipse map of highest entropy. The space of parameters is well behaved with a single, well defined entropy maximum in each case. R_d is best constrained in outburst, while β is better constrained in quiescence: the entropy of the eclipse maps drops quickly for $R_d < 0.75 R_{L1}$ in outburst, and for $\beta > 1.0^{\circ}$ in quiescence. The accretion disc fills the primary Roche lobe at outburst ($R_d = 0.85 R_{L1} = 0.36 R_{\odot}$). It shrinks to $0.6 R_{L1} (= 0.25 R_{\odot})$ during decline and reaches $0.45 R_{L1} (= 0.19 R_{\odot})$ in quiescence³. These results are in line with the qualitative inferences drawn in Sect. 3.1 and in agreement with the $\simeq 0.4 R_{L1}$ quiescent disc radius found by Borges & Baptista (2005). There is marginal evidence that the disc half-opening angle is larger in outburst ($\beta = 1.0^{\circ} \pm 0.5^{\circ}$) than in quiescence ($\beta = 0.5^{\circ} \pm 0.5^{\circ}$). The disc is geometrically thin in all three cases.

In order to check the consistency of the inferred R_d values, we applied the method described by Sulkanen et al. (1981) to estimate the disc radius from the half-width of the eclipse $\Delta\phi_E$. By assuming a spherical secondary star it is possible to derive the disc radius R_d in units of the orbital separation a from the analytical expression,

$$\frac{R_d}{a} = \sin(2\pi\Delta\phi_E) \sin i - \sqrt{(R_2/a)^2 - \cos^2 i}, \quad (2)$$

where R_2/a is the radius of a sphere containing the same volume as the Roche lobe of the secondary star, given by the relation (Eggleton 1983),

$$\frac{R_2}{a} = \frac{0.49 q^{2/3}}{0.6 q^{2/3} + \log(1 + q^{1/3})}. \quad (3)$$

Values of R_d/a are transformed to R_d/R_{L1} assuming $a/R_{\odot} = 0.61 \pm 0.05$ (Borges & Baptista 2005). Measurements of $\Delta\phi_E$ were obtained by fitting a spline function to the out-of-eclipse phases of each light curve, finding the phases where the fitted spline deviates from the data by 1σ of the local, out-of-eclipse median flux, and dividing the resulting phase range by two. We find $\Delta\phi_E$ values of 0.122 ± 0.005 cycle, 0.097 ± 0.005 cycle and 0.076 ± 0.005 cycle, respectively for the outburst, decline and quiescence light curves. These measurements lead to corresponding disc radii of $R_d/R_{L1} = 0.79 \pm 0.08$, 0.62 ± 0.07 , and 0.45 ± 0.06 , in very good agreement with the values derived from the entropy landscape procedure. The measured ingress/egress eclipse phases are depicted as pairs of vertical tick marks in the left-hand panels of Fig. 3.

We used the expression of Hessman & Hopp (1990)

³ The uncertainty is $0.05 R_{L1} = 0.021 R_{\odot}$ in each case.

to compute a circularization radius (the smallest possible radius for an inviscid accretion disc) of $R_{\text{circ}}/R_{\text{L1}} = 0.0859 q^{-0.426} (R_{\text{L1}}/a)^{-1} = 0.30$. Thus, the measured quiescent disc radius of V4140 Sgr is larger than its circularization radius at a 3σ confidence level.

3.3.2 Evolution of disc surface brightness

Eclipse maps corresponding to the best-fit (R_d, β) values are shown in Fig. 3, together with the data and model light curves. The orientation of the eclipse maps is such that the secondary star rotates counter-clockwise around the WD at the centre of the map (in the observer’s reference frame), while the observer rotates clockwise (in the binary reference frame). At phase zero, the secondary and the observer are on the right side of the map (with the projected shadow of the secondary star covering most of the disc). At phase $+0.25$ cycle the observer is at the bottom (in the binary frame) while the secondary star is at the top of the eclipse map (in the observer’s frame).

The inner disc regions remain roughly at the same brightness level through outburst, while significant brightness changes take place in the outer disc regions. In order to emphasize these changes and the brightness asymmetries in the outer disc regions, the inner disc regions of the eclipse maps ($R < 0.35 R_{\text{L1}}$) were masked in the middle-right panels of Fig. 3.

At outburst, the surface brightness distribution of the outer disc is skewed towards the L1 point indicating that the disc is elliptical at this stage. Two dotted circles are overplotted on the eclipse map to help visualize the elliptical disc brightness distribution. The outer circle corresponds to the disc rim $R_{\text{max}} = R_d = 0.85 R_{\text{L1}}$, while the inner circle has $R_{\text{min}} = 0.65 R_{\text{L1}}$. From these radii we estimate a disc eccentricity $e = (R_{\text{max}} - R_{\text{min}})/(R_{\text{max}} + R_{\text{min}}) = 0.13$. For our outburst dataset the phase of superhump maximum coincides with mid-eclipse, right when the bulge of the elliptical disc is aligned with the secondary star. Although less conspicuous, a similar brightness asymmetry is also present in the decline eclipse map. In this case the major axis of the ellipse is oriented at an angle $\simeq 100^\circ$ with respect to the line joining both stars, implying that the alignment of the secondary star with its bulge occurs at binary phase $\simeq +0.28$ cycle. This is in good agreement with the observed phase of superhump maximum in the decline light curve, $\phi_{\text{max}} = +0.25$ cycle. From this eclipse map we find $R_{\text{max}} = R_d = 0.6 R_{\text{L1}}$ and $R_{\text{min}} = 0.45 R_{\text{L1}}$, also leading to a disc eccentricity $e = 0.13$.

These results are in line with the tidal resonance instability model, which explains superhumps in terms of enhanced tidal dissipation (and extra disc emission) as the secondary star passes closer to the bulge of a slowly precessing elliptical disc (Whitehurst 1988; Hirose & Osaki 1990; Lubow 1991, 1994). For V4140 Sgr, the 3:1 resonance radius is $R_{31} = 0.66 R_{\text{L1}}$. At outburst, the disc is comfortably larger than R_{31} ($R_d = 0.85 R_{\text{L1}}$), whereas in the decline dataset the disc radius is slightly smaller than R_{31} ($R_d = 0.6 R_{\text{L1}}$). The measured disc eccentricities are in good agreement with the $e \simeq 0.1$ value found in numerical simulations of the tidal resonance instability by Hirose et al. (1991).

Since the timescale of disc precession ($\simeq 2$ -3 days, see Table 3.3 of Warner 1995) is much longer than P_{orb} , the change in orientation of the elliptical disc along the time

span of the outburst and decline datasets ($\simeq 3$ h) is $\Delta\theta \leq 20^\circ$, smaller than the azimuthal smearing effect adopted for the maximum entropy reconstructions ($\Delta\theta = 30^\circ$). Therefore, there is no significant azimuthal ‘blurring’ of the outburst and decline eclipse maps caused by the slow precession of the elliptical disc.

The right-hand panels of Fig. 3 show the brightness distributions along the disc rim. A word of caution is on demand before we attempt to interpret these distributions. One of the basic assumptions of the eclipse mapping method is that the intensities in the eclipse map are independent of binary phase, and that all changes in the light curve are caused by variable visibility and/or aspect of pixels with phase. Superhumps clearly violate this assumption if they correspond to true, physical changes in intensity of accretion disc regions with binary phase. Therefore, the disc rim intensity distributions in outburst and decline should not be interpreted as if there is enhanced emission from extended regions at disc rim. Instead, they just signal the azimuths (or binary phases) where enhanced emission from the superhump light source occurs in each light curve. Thus, the disc rim distributions tell us that superhump emission is produced over a large fraction of the orbital period and is centred at phase $\phi_{\text{max}} = 0$ and $+0.25$ in outburst and decline, respectively (of course, this can also be inferred by direct inspection of the corresponding light curves). However, an additional useful information is that, aside of the elliptical disc bulge (responsible for the disc rim emission at azimuth $\theta_{\text{sh}} \simeq 0$), there are two other superhump light sources in outburst, at azimuths $\theta_{\text{sh}} \simeq \pm(80^\circ - 90^\circ)$ – when the secondary star is roughly orthogonal to the major axis of the elliptical disc. A similar inference can be drawn from the decline disc rim distribution, although in this case the two sources are closer in azimuth than in outburst and the disc bulge contribution seems considerably reduced or blended in azimuth with that from the two side sources. These results are reminiscent to those of O’Donoghue (1990). He applied a modified eclipse mapping technique to investigate the superhump light source in Z Cha when superhump maximum is centred in eclipse, and found that the extra emission arises from three sources in the outer disc regions, one towards the L1 point and two sources symmetrically located in the orthogonal directions. These orientations coincide with the predicted positions where the elliptical orbits intersect (Hellier 2001).

Let us turn our attention to the quiescence light curve. Its eclipse map is dominated by emission from an extended asymmetric source with no distinguished contribution from the WD (i.e., no sharp ingress/egress features in eclipse shape), indicating that efficient accretion through a high-viscosity disc is taking place in quiescence. The long egress shoulder in the eclipse shape translates into enhanced emission along the outer disc regions ahead of the stream-disc impact point, suggesting inefficient downstream cooling in the disc flow (Smak 1971). On the other hand, the weak orbital hump maps into a disc rim narrow spot ($\Delta\theta = 40^\circ$) at zero azimuth. The apparent hump phase of maximum $\phi_{\text{max}} = -0.08$ cycle is an illusion, as the spot starts being eclipsed together with the accretion disc soon after that phase and is behind the shadow of the secondary star when seen face on. The azimuth of maximum emission of this spot ($\theta_{\text{max}} = 0^\circ$) does not coincide with the radial direction of

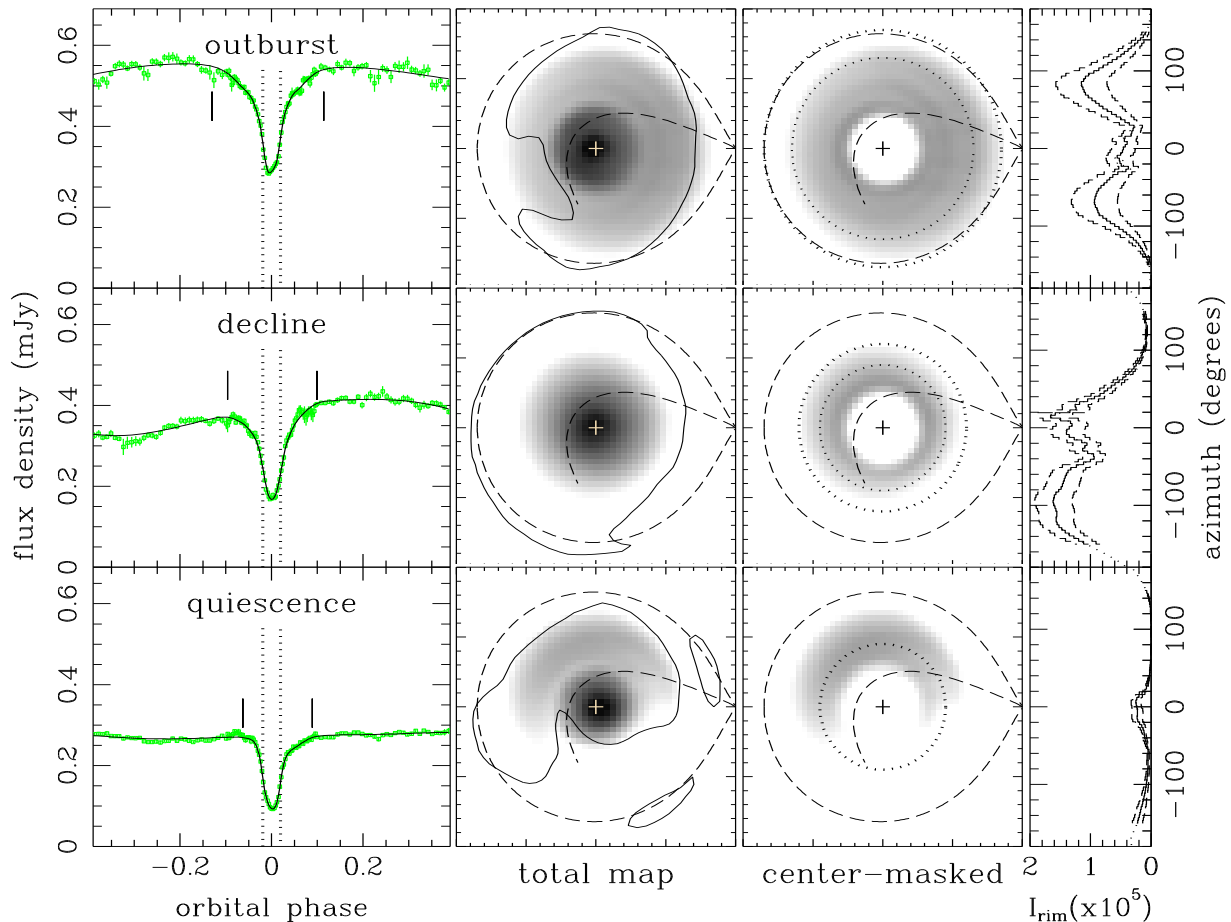


Figure 3. Left-hand: Data (points with error bars) and model (solid lines) light curves for the outburst, decline and quiescence states. Vertical dotted lines mark the ingress/egress phases of the WD, while vertical tick marks depict the phases of eclipse ingress/egress (see text). Middle-left: the corresponding eclipse maps in a logarithmic grayscale (dark regions are brighter). A cross marks the position of the WD at disc centre. Dashed lines depict the primary Roche lobe and the gas stream trajectory. A contour line for $S/N=3$ is overplotted on each map; features in the eclipse maps are statistically significant at or above the 3σ level. The stars rotate counter-clockwise. Middle-right: the eclipse maps with their central regions ($R < 0.35 R_{L1}$) masked for a clearer view of the brightness distribution at the outer disc regions. Dotted circles mark the minimum radius that matches the asymmetric outer disc brightness distribution (for the outburst and decline maps) and the best-fit disc rim radius. Right-hand: the intensity distribution along the disc rim. Dashed lines show the 1σ limit on the intensity distribution. Azimuths are counted from the line joining both stars and increase counter-clockwise.

the stream-disc impact point ($\theta = 31^\circ$), but with the direction of the infalling gas stream at that point. This is in contrast with results from the dwarf novae U Gem (Marsh 1988), OY Car (Wood et al. 1989) and IP Peg (Ribeiro et al. 2007), where the maximum emission of the quiescent bright spot lies in the direction normal to a plane roughly midway between the disc and stream flows.

3.3.3 Radial temperature distributions

In the DIM framework, a dwarf nova accretion disc cycles between a hot, high-viscosity state where hydrogen is fully ionized (outburst) and a faint, low-viscosity state where hydrogen is mostly neutral (quiescence) (Lasota 2001; Frank et al. 2002). The instability that sets this limit-cycle behavior is tied to the partial ionization of hydrogen – which leads to tight constraints in disc gas temperature along the outburst cycle. Namely, there is a critical effective temperature $T_{\text{crit}2}$

above which the disc gas should stay while in outburst, and a critical effective temperature $T_{\text{crit}1}$ below which it should remain while in quiescence (Lasota 2001),

$$T_{\text{crit}1} = 5800 \left(\frac{M_1}{M_\odot} \right)^{0.03} \left(\frac{R}{10^{10} \text{ cm}} \right)^{-0.09} \text{ K}, \quad (4)$$

$$T_{\text{crit}2} = 7200 \left(\frac{M_1}{M_\odot} \right)^{0.03} \left(\frac{R}{10^{10} \text{ cm}} \right)^{-0.08} \text{ K}. \quad (5)$$

Decline from outburst is understood in terms of the inwards propagation of a cooling front from the outer disc regions, progressively transitioning the disc from its hot state back to the cool quiescent state. Disc regions ahead of the cooling front should still have $T > T_{\text{crit}2}$, while those behind the cooling front should show $T < T_{\text{crit}1}$.

This prediction can be tested with eclipse mapping. If the distance to the binary is known, the usual practice is to convert the intensities in the eclipse maps to blackbody

brightness temperatures T_b , which can then be compared to T_{crit} and to the $T_{\text{eff}}(R) \propto R^{-3/4}$ law of opaque, steady-state disc models. A valid criticism about this procedure is that T_b may not be a proper estimate of the disc effective temperature T_{eff} . As pointed out by [Baptista et al. \(1998\)](#), a relation between these two quantities is non-trivial, and can only be properly obtained by constructing self-consistent models of the vertical structure of the disc. On the other hand, observations indicate that the colors of optically thick disc regions are in between those of blackbody and main-sequence stars ([Horne & Cook 1985](#); [Horne & Stiening 1985](#); [Bruch et al. 1996](#); [Baptista et al. 1996](#)) – in which cases a broad-band, blackbody brightness temperature becomes a fair and useful approximation to T_{eff} . [Borges & Baptista \(2005\)](#) applied a method similar to cluster main-sequence fitting to an accretion disc color-magnitude diagram of V4140 Sgr to infer a distance of 170 ± 30 pc. Their eclipse maps lead to radial brightness temperatures in outburst and quiescence which are consistent at the 1σ limit in the B , V and R passbands, suggesting that the accretion disc is indeed optically thick and that $T_b \simeq T_{\text{eff}}$ is a reasonable approximation in this case.

Fig. 4 shows azimuthally-averaged radial brightness temperature distributions for the outburst (solid squares), decline (crosses) and quiescence (open squares) accretion disc maps for assumed distances of 170 pc (bottom) and 260 pc (top, the upper 3σ limit on the distance estimate of [Borges & Baptista 2005](#)). The intensities in the eclipse maps were scaled to the assumed distances and corrected for interstellar extinction effects before being converted to brightness temperatures. From the galactic interstellar contour maps of [Lucke \(1978\)](#), we estimate a reddening of $E(B - V) = 0.4 \text{ mag kpc}^{-1}$ towards the direction of V4140 Sgr.

The temperatures in the inner disc regions ($R < 0.1 R_{\text{L1}}$) are consistently the same throughout outburst. The outer disc regions ($R > 0.1 R_{\text{L1}}$) progressively cool from outburst to quiescence. At a distance of 170 pc the whole outburst cycle proceeds at temperatures below $T_{\text{crit}2}$. Increasing the distance to the binary increases the intrinsic intensities and corresponding disc brightness temperatures. But even at a distance of 260 pc most disc regions ahead of the inwards moving cooling wave show temperatures below $T_{\text{crit}2}$. In order to reconcile the observations with DIM, one needs to increase the distance above 300 pc. However, this steepens the radial temperature distribution in quiescence, bringing it into good agreement with the $T \propto R^{-3/4}$ law of high-viscosity, opaque steady-state discs – in contradiction to the DIM expectation that quiescent disc of dwarf novae should have low viscosities ($\alpha \sim 0.01$), long viscous timescales and, therefore, would hardly have time to reach a steady-state in between consecutive outbursts. Furthermore, this also increases the disc temperatures in quiescence, bringing an increasing (and significant) fraction of the quiescent disc into contradiction with the DIM requirement $T < T_{\text{crit}1}$. In other words, the disc temperatures do not differ sufficiently in outburst and quiescence that one can have both $T < T_{\text{crit}1}$ everywhere in quiescence and $T > T_{\text{crit}2}$ over most of the disc in outburst. It seems clear that *it is not possible to reconcile the outbursts of V4140 Sgr with DIM.*

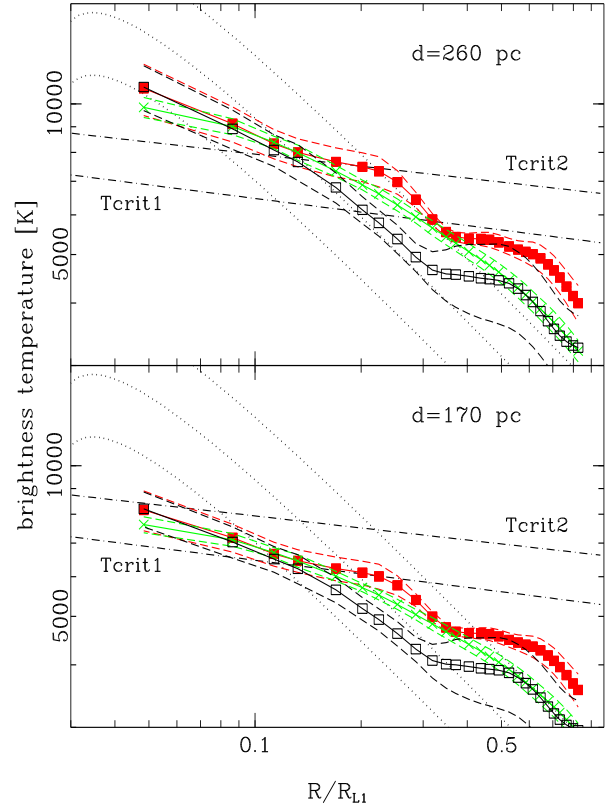


Figure 4. Azimuthally-averaged radial brightness temperature distributions for the outburst (solid squares, red), decline (crosses, green) and quiescence (open squares, black) accretion disc maps, for radial bins of width $0.03 R_{\text{L1}}$. Dashed lines show the 1σ limits on the average temperatures. Dotted lines correspond to steady-state optically thick disc models for mass accretion rates of 10^{-10} , $10^{-10.5}$ and $10^{-11} M_{\odot} \text{ yr}^{-1}$, respectively from top to bottom. Dot-dashed lines show the critical effective temperatures $T_{\text{crit}2}$ (above which the disc gas should stay while in outburst) and $T_{\text{crit}1}$ (below which it should remain while in quiescence), according to the DIM (e.g., [Warner 1995](#)). The distributions are shown for assumed distances of 260 pc (top) and 170 pc (bottom).

3.4 Flickering mapping in quiescence

Figure 5 shows the individual quiescent light curves of V4140 Sgr superimposed in phase. Along the $\simeq 50$ d time interval covered by the quiescence observations, V4140 Sgr showed no systematic change or long-term trend in eclipse depth, out-of-eclipse brightness or eclipse width. Therefore, the light curves of that period can be assigned to a single brightness state, and all observed variability can be attributed to flickering. The top panel depicts light curves of a comparison star of similar brightness. The scatter with respect to the mean flux is perceptibly larger in V4140 Sgr than in the comparison star and is caused by flickering. The scatter is larger close to orbital hump maximum (suggesting that the bright spot contributes to the flickering) and is smaller during eclipse (indicating that flickering sources are occulted at these phases).

We applied the “single” ([Bruch 1996, 2000](#)) and “ensem-

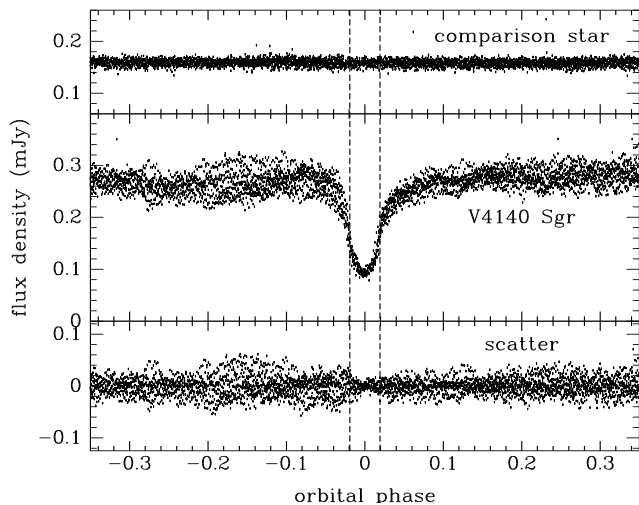


Figure 5. The quiescent light curves of V4140 Sgr (middle) and of a comparison star of similar brightness (top). The lower panel shows the light curves of the middle panel after subtraction of the average orbital curve; the scatter around the mean flux yields an indication of the flickering amplitude at each phase. Vertical dashed lines mark the ingress/egress phases of the WD.

ble” (Horne & Stiening 1985; Bennie et al. 1996) techniques to the quiescent light curves of V4140 Sgr to derive the orbital dependency of its steady-light and of the low- and high-frequency flickering components. The reader is referred to Baptista & Bortoletto (2004) for a detailed description and combined application of both techniques. While the ensemble technique samples flickering at all frequencies, the typical power law dependency of the flickering in CVs implies that an ensemble curve is dominated by the low-frequency flickering components. On the other hand, the high-pass filtering process of the single technique leads to curves which sample the high-frequency flickering. The combination of both methods allows one to separate the low- (ensemble) and high-frequency (single) components of the flickering sources.

Because all light curves are at the same brightness level, applying the ensemble technique becomes a matter of computing the mean flux at each phase bin (the steady-light curve) and the standard deviation with respect to the mean (the scatter curve, $\sigma_{\text{tot}}(\phi)$, with contributions from the Poisson noise, $\sigma_{\text{Poi}}(\phi)$, and from the flickering, $\sigma_{\text{flick}}(\phi)$). The angular coefficient (which measures the long-term brightness changes) is consistently zero within the uncertainties. The ensemble flickering curve is obtained by correcting the scatter curve from the Poisson noise contribution,

$$\sigma_{\text{flick}}(\phi) = \sqrt{\sigma_{\text{tot}}^2(\phi) - \sigma_{\text{Poi}}^2(\phi)}. \quad (6)$$

The average steady-light curve was subtracted from each individual light curve to remove the DC component, and a Lomb-Scargle periodogram (Press et al. 1992) was calculated. The periodograms of all light curves were combined to yield a mean periodogram and a standard deviation with respect to the mean. Figure 6 shows the resulting average power density spectrum (PDS) binned to a resolution of 0.02 units in log(frequency). The PDS is well described by a power law $P(f) \propto f^{-1.2}$, which becomes flat for $f_{\text{low}} < 0.2$ mHz ($t_{\text{low}} > 83$ minutes) and disappears in the

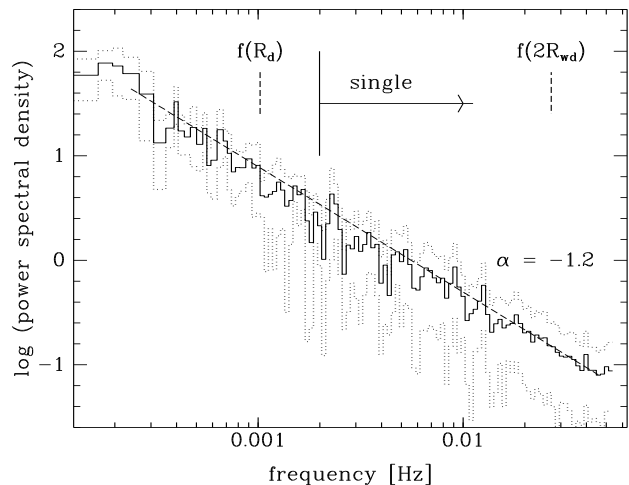


Figure 6. Average PDS. Dotted lines show the 1σ limits on the average power. The best-fit power law $P(f) \propto f^{-1.2}$ is shown as a dashed line. A vertical tick marks the low-frequency cut-off of the filtering process applied to derive the single scatter curve. The Keplerian frequencies corresponding to $2R_{\text{wd}}$ and to the quiescent disc radius R_d are illustrated as vertical dashed ticks.

white noise for $f_{\text{high}} > 40$ mHz ($t_{\text{high}} < 25$ s). The slope of the PDS distribution is consistent with the general trend found in other CVs, which can be well described by power laws with average exponent $P(f) \propto f^{-2.0 \pm 0.8}$ (Bruch 1992; Baptista & Bortoletto 2004, 2008).

We followed Baptista & Bortoletto (2008) and subtracted the average steady-light curve from each individual light curve before applying the single filtering process in order to eliminate the steep gradients produced by the eclipse in the light curve. Our single light curve includes flickering components with frequencies $f_c > 2$ mHz (timescales shorter than 500 s). Single curves obtained with higher cut-off frequencies show the same morphology but are noisier (because of the reduced power) and lead to less reliable results, while for those obtained with lower cutoff frequencies the excess of filtering starts smearing out the eclipse of the flickering. The single flickering curve is obtained by correcting the corresponding scatter curve from the Poisson noise contribution (cf. Eq. 6).

As the disc opening angle in quiescence is negligible ($\beta = 0.5^\circ$, Sect. 3.3.1), the steady-light and the flickering curves were analyzed by a standard eclipse mapping algorithm (Baptista & Steiner 1993), with a flat Cartesian grid of 51×51 pixels centred on the WD and side $2R_{L1}$ in the orbital plane, to solve for a map of the disc surface brightness distribution in each case. Because this version of the eclipse mapping method does not take into account out-of-eclipse brightness changes, these were removed from the light curves by fitting a spline function to the phases outside eclipse, dividing the light curve by the fitted spline, and scaling the result to the spline function value at phase zero.

The adopted eclipse geometry ($\Delta\phi, q, i$) and default map parameters ($\Delta r, \Delta\theta$) are the same as in Sect. 3.3, and the reconstructions also reached a final reduced chi-square $\chi_{\text{red}}^2 \simeq 1$ in all cases. Monte Carlo simulations with the bootstrap technique were similarly performed to obtain the uncertainties in the eclipse maps. These are used to draw the

contour maps of Fig. 7, and to estimate the uncertainties in the radial distributions shown in Fig. 8.

The resulting steady-light, ensemble and single curves have phase resolution of 0.003 cycle and cover the phase range $(-0.15, +0.15)$ cycle. These light curves and corresponding eclipse maps are shown in Fig. 7.

3.4.1 The steady-light

The steady-light curve is the quiescence light curve of Sect. 3.3 after removal of the weak orbital hump. Consistently, the steady-light eclipse map is very similar to the quiescence eclipse map (Fig. 3), showing a broad brightness distribution of an asymmetric accretion disc which extends up to $0.45 R_{L1}$. This brightness distribution was already discussed in Sect. 3.3.2.

It is worth noting that, although derived from essentially the same light curve, the steady-light map is of higher statistical significance than its cousin quiescence map. This reflects a subtle but relevant difference between the standard and the 3D eclipse mapping. Standard eclipse mapping is simpler and more robust to noise in the light curve (e.g., flickering) as only a relatively narrow phase range of the light curve covering the eclipse shape is used to derive the disc brightness distribution. Because 3D eclipse mapping uses the whole orbital light curve to derive the disc + rim brightness distributions, it is more sensitive to noise in the light curve and any flare/flicker outside of eclipse contributes to the uncertainty of all visible pixels at that phase. Nevertheless, the intrinsic lower statistical significance of the 3D eclipse mapping seems a reasonable price to pay in return for the extra information about the disc radius and half-opening angle delivered by this technique. On the other hand, the higher statistical significance with which maps are obtained with the standard eclipse mapping is key to allow statistically meaningful results in the derivation of the radial distribution of the flickering amplitude (Sect. 3.4.2).

3.4.2 low- and high-frequency flickering

The ensemble and single flickering curves have similar shapes, showing the deeper eclipse of a central source plus an extended egress shoulder. This eclipse shape maps into an asymmetric source along the disc rim ahead of the stream-disc impact point ($R \simeq 0.45 R_{L1}$, stream-disc impact flickering) and an extended central source several times larger in radius than the WD at disc centre (boundary layer + disc-related flickering)⁴. The solid contour line overplotted on each eclipse map depicts the 3σ confidence level region as derived from the map of statistical significance in each case. The two flickering sources are statistically significant at or above the 3σ confidence level both in the ensemble and in the single map.

The disc-related flickering component is not centred at the WD position, but is slightly skewed towards the ballistic stream trajectory. We tested whether this was an artifact caused by an error in the choice of phase zero by obtaining

eclipse maps for versions of the light curves with small offsets in phase and by allowing changes in the adopted eclipse geometry within the uncertainties in the binary parameters q and i . These simulations indicate that it is not possible to simultaneously centre the steady-light brightness distribution and the disc flickering component, and we conclude that the slight offset of the disc flickering component is real.

Azimuthally-averaged radial intensity distributions for the steady-light, ensemble and single flickering maps are shown in the right-hand panels of Fig. 7. Each eclipse map is separated in radial bins of width $0.03 R_{L1}$ and the median intensity is computed for each bin. The associated uncertainty is obtained by computing the median absolute deviation with respect to the median intensity for the set of bootstrap reconstructions of the corresponding map and multiplying the result by 1.48 to find the standard deviation (e.g., Hoaglin et al. 1983).

Fig. 8a compares the relative amplitude of the ensemble and single flickering in V4140 Sgr. The radial run of the relative amplitudes are obtained by dividing the radial intensity distribution of these two flickering maps by that of the steady-light. Dashed lines show the 1σ limits on the average flickering amplitudes. The distributions are not reliable for $R > 0.5 R_{L1}$ because of the reduced statistical significance of the flickering maps and the rapidly declining intensities in the steady-light map, and are not shown in Fig. 8a.

The difference between the ensemble and single distributions tells us where the low-frequency flickering comes from. An excess of ensemble over single flickering at $R \leq 0.12 R_{L1} \simeq 5 R_{wd}$ indicate the existence of a low-frequency flickering central source at the 2.5σ confidence level. The radial extent of this source is too large to be accounted for by the radial smearing effect of the entropy on the eclipse map⁵ (see Baptista et al. 1996), indicating that the source is larger than the WD by a factor $\simeq 2 - 3$. This central flickering component may possibly arise from optical reprocessing of intermittent x-ray and UV irradiation by the boundary layer at the atmosphere of the innermost disc regions. Additional excess of ensemble over single flickering is seen in the outer disc regions ($R > 0.4 R_{L1}$, at the 3σ confidence level), which is readily associated to the stream-disc impact region. This stream-disc flickering component is relatively stronger ($\simeq 5$ per cent amplitude) than the central source flickering ($\simeq 3$ per cent amplitude). There is no low-frequency flickering produced in the intermediate disc regions ($0.12 < R/R_{L1} < 0.4$). The high-frequency flickering is spread over the accretion disc, with a $\simeq 4 - 5$ per cent amplitude roughly independent of disc radius. This is the disc-related flickering component. The slight increase in high-frequency flickering amplitude at the innermost and outer disc regions might be due to some high-frequency contribution from the central and stream-disc flickering components.

Our ensemble and single flickering maps allow us to disentangle three different sources of flickering in V4140 Sgr. The presence of a central flickering and of a stream-disc impact flickering sources are in good agreement with the scenario put forward by Bruch (1992, 2000). If the central flickering component arises in the boundary layer its spectrum

⁴ A small circle at the centre of each eclipse map depicts the size of the WD to allow a direct comparison with the radial extent of the disc-related flickering component.

⁵ In our eclipse maps, point sources are smeared in the radial direction by $3 \Delta r = 0.06 R_{L1} \simeq 2.4 R_{wd}$.

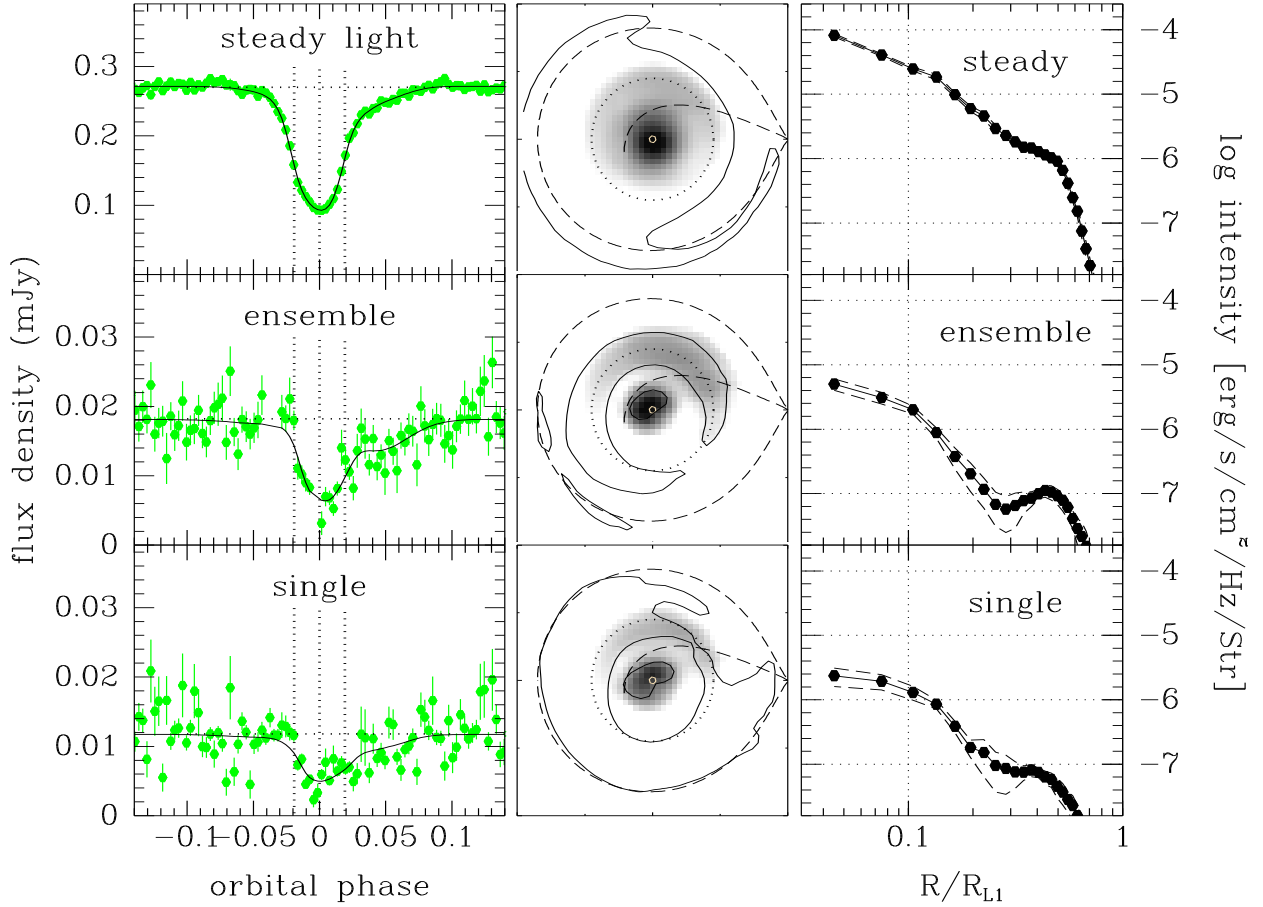


Figure 7. Left: Data (points with error bars) and model (solid lines) light curves for the steady-light, the ensemble and the single flickering curves. Vertical dotted lines mark the ingress/egress phases of the WD and mid-eclipse. Middle: the corresponding eclipse maps in a logarithmic grayscale (dark regions are brighter). A small circle marks the position and size of the WD at disc centre. The notation is the same as in Fig. 3. Features in the eclipse maps are statistically significant at or above the 3σ level. Right: Azimuthally-averaged radial intensity distributions of the eclipse maps in the middle panels. Dashed lines show the 1σ limits on the average intensities.

may be much bluer than the inner disc spectrum, and our optical flickering mapping experiment is underestimating its contribution to the total flickering. In this case, this boundary layer flickering should dominate the UV light curve of V4140 Sgr, with fast reduction in flickering activity as the WD goes into eclipse. Our flickering mapping experiment also reveals the existence of a disc flickering component in V4140 Sgr, which allow us to probe the viscosity in its quiescent disc (see Sect. 4). This disc flickering component accounts for 2/3 of the total optical flickering in V4140 Sgr. The results bear some resemblance with those from the quiescent dwarf nova V2051 Oph, where the low-frequency flickering is associated with an overflowing gas stream while the high-frequency flickering arises from the accretion disc (Baptista & Bortoletto 2004).

4 THE QUIESCENT DISC VISCOSITY

The identification of a disc-related flickering component enables us to follow the steps of Baptista & Bortoletto (2004) and to use the model of Geertsema & Achterberg (1992) to estimate the magnitude of the viscosity parameter α for the

quiescent disc of V4140 Sgr. This allows us to critically test the largely different predictions of DIM and MTIM for a quiescent disc of a dwarf nova. As the expression relating α and $\sigma_D/\langle D \rangle$ involves the disc relative thickness H/R and because this quantity is loosely constrained by the entropy landscape analysis, we start our exercise by using the measured radial temperature distribution for an independent (and more precise) measurement of H/R as well as to check the consistency of the thin disc result of Sect. 3.3.1.

In the atmosphere of an opaque, α -disc model,

$$T_c^{1/2} = s T_{\text{eff}}^{1/2} \simeq s T_b^{1/2}, \quad (7)$$

where T_c is the mid-plane disc temperature, s is the square root of the mid-plane to the effective temperature ratio and the final step is justified by the discussion in Sect. 3.3.3. An estimate of the s value is obtained by comparing the analytical fits of the critical effective temperatures ($T_{\text{crit1}}, T_{\text{crit2}}$) and of T_c (see, e.g., eqs. A5-A8 in Lasota 2001); for the upper turning point ($\alpha \sim 0.1$), $s = (T_c/T_{\text{crit2}})^{1/2} \simeq 2$, while for the lower turning point ($\alpha \sim 0.01$), $s = (T_c/T_{\text{crit1}})^{1/2} \simeq 1.5$. Hirose et al. (2014) computed detailed equilibrium vertical atmospheres of α -discs subject to MHD turbulence for a set of physical conditions of interest to dwarf nova acce-

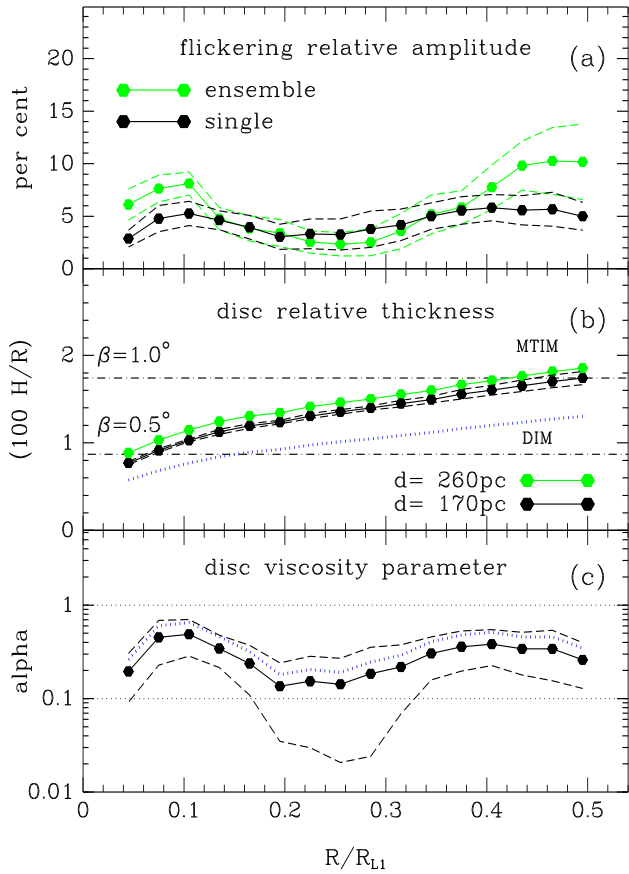


Figure 8. Azimuthally-averaged radial distributions. (a) The relative amplitude of the ensemble and single flickering. Dashed lines show the 1σ limits on the average values. (b) The disc relative thickness (H/R) derived from the $T_b(R)$ distribution assuming $s = 2$ (MTIM case) for distances of 170 pc (black) and 260 pc (green). Dashed lines show the 1σ limits on the H/R distribution derived from the uncertainties in the $T_b(R)$ distribution. The dotted line corresponds to the H/R distribution assuming $s = 1.5$ (DIM case). Horizontal dot-dashed lines depict the H/R value derived from the measured disc half-opening angle (Sect. 3.3.1) and its 1σ upper limit. (c) The disc viscosity parameter α derived using the Geertsema & Achterberg (1992) model. The solid line corresponds to the H/R distribution for the MTIM case ($s = 2$); dashed lines show the 1σ limits on the derived α value. A dotted line depicts the corresponding distribution for the DIM case ($s = 1.5$).

tion discs. Their model for a high-viscosity ($\alpha \simeq 0.1$), hot and opaque disc with $T_{\text{eff}} = 7490 \text{ K}$ (representative of the range of disc temperatures found in V4140 Sgr) consistently has $T_c = 4T_{\text{eff}}$ (or $s = 2$). Thus, we adopt $s = 2$ for the case of a high-viscosity quiescent disc (as expected in the MTIM framework) and we take $s = 1.5$ as corresponding to a low-viscosity quiescent disc (as expected in the DIM framework).

We may then use the inferred $T_b(R)$ distribution and the thin disc approximation to estimate the radial run of the relative disc thickness H/R (Frank et al. 2002),

$$\frac{H}{R} = \frac{c_s}{v_k} = \left(\frac{kT_c}{\mu m_H} \frac{R}{GM_{\text{wd}}} \right)^{1/2} \propto s [RT_b(R)]^{1/2}, \quad (8)$$

where k and G are, respectively, the Boltzmann and the gravitation constants, μ is the mean molecular weight, m_H is the hydrogen atom mass, and we adopt $\mu = 0.615$ (adequate for a fully ionized ‘cosmic’ mixture of gases), $M_{\text{wd}} = 0.73 \pm 0.08 M_\odot$ (Borges & Baptista 2005). The disc relative thickness obtained with Eq.(8) assuming $s = 2$ (MTIM case) is plotted in Fig. 8b for distances of 170 pc (black) and 260 pc (green). An H/R distribution computed assuming $s = 1.5$ (DIM case) and distance of 170 pc is shown as a dotted line in Fig. 8b. The uncertainties in the H/R distribution are dominated by the uncertainty in the temperature scaling factor s . For a given T_{eff} value, a quiescent DIM disc is thinner than its MTIM counterpart because its mid-plane temperature is lower and, therefore, c_s and H are also lower. The fact that the H/R distributions increase with radius imply that the disc face is concave and, therefore, there is room for reprocessing of x-ray and UV radiation from the boundary layer in the disc atmosphere (e.g., Frank et al. 2002, see Sect. 3.4.2). The disc relative thickness derived from the disc half-opening angle ($\tan \beta = H/R = 0.0087 \pm 0.0087$) is shown as horizontal dot-dashed lines for comparison. Disc relative thicknesses derived independently from the disc temperatures and from the disc half-opening angle are consistent with each other at the 1σ level, and indicate that the quiescent disc of V4140 Sgr is geometrically thin.

Once we have the radial runs of the relative amplitude of the disc flickering and of the disc thickness, we may use the MHD turbulence model of Geertsema & Achterberg (1992) to estimate the radial run of the viscosity parameter in the quiescent disc of V4140 Sgr. In their model, the number of turbulent eddies that contribute to the local fluctuation is,

$$N(R) = 4\pi \frac{R}{H} \left(\frac{H}{L} \right)^2, \quad (9)$$

where L is the size of the largest turbulent eddy. The local rms value of the fluctuations $\sigma_D(R)$ in the average energy dissipation rate per unit area $\langle D(R) \rangle$ is found to be,

$$\sigma_D(R) \simeq 2.5 \langle D(R) \rangle / \sqrt{N(R)}, \quad (10)$$

while the disc viscosity parameter can be written as,

$$\alpha \equiv \frac{\langle T_{r\phi} \rangle}{P} = \frac{3\nu_t}{2c_s H} \simeq 0.9 \left(\frac{L}{H} \right)^2, \quad (11)$$

where $\langle T_{r\phi} \rangle$ is the local average shear stress (Maxwell + Reynolds), P is the local pressure, and ν_t is the local (turbulent) disc viscosity. Combining Eqs. (9-11), we obtain the radial run of the disc viscosity parameter,

$$\alpha(R) \simeq 0.46 \left[\frac{100 H}{R} \right]^{-1} \left[\frac{\sigma_D(R)}{0.05 \langle D(R) \rangle} \right]^2. \quad (12)$$

If the disc-related flickering is caused by fluctuations of the energy dissipation rate induced by MHD turbulence in an optically thick disc, the relative amplitude of this disc flickering component yields a good estimate of the ratio $\sigma_D/\langle D \rangle$.

The resulting $\alpha(R)$ distributions are shown in Fig. 8c. Because of the dependency $H/R \propto T_b^{1/2}$, the influence of errors in distance and temperature on α is negligible. Errors in s also have a relatively small effect to the uncertainty of α in comparison with the large contribution of the errors in the flickering relative amplitude curves (because of the dependency $\alpha \propto [\sigma_D/\langle D \rangle]^2$ and the relatively lower accuracy of the latter quantity). Large values of $\alpha \simeq 0.2 - 0.4$

at found all disc radii, in good agreement with the MTIM expectations. In order to model the long (80-90 d) time interval between outbursts of V4140 Sgr in the DIM framework, an $\alpha_{\text{quies}} \simeq 0.01$ is required (Cannizzo 1993; Warner 1995; Lasota 2001). This corresponds to the lower y-axis end of Fig. 8c. The derived α 's are systematically larger than the DIM expectation by at least an order of magnitude. Outside the region $0.2 \leq R/R_{L1} \leq 0.3$, the discrepancy is significant at the 2σ limit. Computing $\alpha(R)$ from the H/R distribution of the DIM case ($s = 1.5$, shown as a dotted line in Fig. 8c) only increases the discrepancy, as the thinner DIM disc leads to even larger α values. If the MHD turbulence model of Geertsema & Achterberg (1992) is correct, the above results indicate that the quiescent accretion disc of V4140 Sgr has high-viscosity.

The V4140 Sgr quiescent data allows an additional test of DIM, which is independent of any MHD turbulence model. One of the Achilles' heel of DIM is the prediction (unmatched by observations) that the average brightness of a dwarf nova should increase between successive outbursts as matter piles up in a low-viscosity quiescent disc, steadily increasing the disc surface density, temperature and, therefore, brightness (e.g., Lasota 2001). In an attempt to overcome the discrepancy, Truss et al. (2004) proposed that the unobserved increase in disc brightness along quiescence could be compensated for by the gradual cooling of a small, hot and high-viscosity inner disc region. Their two-dimensional time-dependent numerical models of dwarf nova accretion discs seem to support this proposal. Could the observed high-viscosity quiescent disc of V4140 Sgr be the gradually cooling hot inner disc region proposed by Truss et al. (2004)?

In an eclipsing dwarf nova, the gradual cooling of a hot inner disc region combined with the simultaneous increase in brightness of the outer regions plus the gradual contraction of a low-viscosity, non-steady quiescent disc should make its eclipse progressively narrower (because of disc shrinkage) and shallower (because of the reduced brightness contrast between inner and outer disc). There is no observational support for any of these effects in our V4140 Sgr quiescent data. The shape, width and depth of the quiescent eclipse is consistently the same within the uncertainties along the $\simeq 50$ d time interval covered by our quiescence observations. This observational window corresponds to more than 50 per cent of the typical V4140 Sgr outburst recurrence time (Borges & Baptista 2005) and started right after the end of a superoutburst. The stability of our observations not only do not support the prediction of Truss et al. (2004), but they also indicate that the quiescent accretion disc of V4140 Sgr is in a steady-state regime. Again, this is in excellent agreement with the picture of a high-viscosity quiescent accretion disc.

If the quiescent accretion disc of V4140 Sgr is already in the high-viscosity regime, there is no room for disc instabilities to set in and it is not possible to explain its outbursts in terms of DIM. Moreover, it is not possible to reproduce its short (5-10 d) outburst length in comparison with the relatively long time interval between successive outburst (80-90 d) in the limit-cycle of the DIM framework since there is no further room to increase α by an order of magnitude from quiescence to outburst. In combination with the observed outburst disc temperatures (below those required by

DIM, $T_b < T_{\text{crit}2}$, Sect. 3.3.3), these results strengthen the conclusion that the outbursts of V4140 Sgr are driven by bursts of mass transfer and not by disc instabilities (c.f., Borges & Baptista 2005).

V4140 Sgr is not the only dwarf nova showing observational evidence for outbursts of mass transfer, but the younger member of an increasing list including V2051 Oph (Baptista & Bortoletto 2004; Baptista et al. 2007), EX Dra and HT Cas (Baptista & Catalán 2001; Baptista 2012), V513 Cas and IW And (Hameury & Lasota 2014), and possibly EX Hya (Hellier et al. 2000).

5 CONCLUSIONS

We applied 3D eclipse mapping techniques to follow the evolution of the surface brightness of the accretion disc of V4140 Sgr in a superoutburst. We find that the disc is elliptical in outburst and decline, with an eccentricity $e = 0.13$. In both outburst stages, the disc orientation is such that superhump maximum occurs when the secondary star is aligned with the bulge of the elliptical disc. This lends observational support for the tidal resonance instability model of superhumps.

The accretion disc fills the primary Roche lobe at outburst ($R_d = 0.85 R_{L1}$), shrinks to $0.6 R_{L1}$ during decline and reaches a lower value of $0.45 R_{L1}$ in quiescence. There is marginal evidence that the disc half-opening angle is larger in outburst ($\beta = 1.0^\circ \pm 0.5^\circ$) than in quiescence ($\beta = 0.5^\circ \pm 0.5^\circ$), but the disc is geometrically thin in all three cases.

The superoutburst occurs at disc temperatures too low to be accounted for by the disc-instability model even at the upper 4σ limit on the inferred distance to the binary. The stability of the eclipse shape, width and depth along 50 d in the quiescent period following the superoutburst and the derived disc surface brightness distribution (outshining any contribution from the white dwarf) indicate that the quiescent accretion disc of V4140 Sgr is in a high-viscosity, steady-state regime.

Flickering mapping of the quiescent data reveal three different sources of flickering in V4140 Sgr: an azimuthally-extended stream-disc impact region at disc rim (statistically significant at the 3σ level) and the innermost disc region (statistically significant at the 2.5σ level), responsible for the low-frequency flickering, and an extended, high-frequency disc component responsible for 2/3 of the total optical flickering in V4140 Sgr. Assuming that the disc-related flickering is caused by fluctuations in the energy dissipation rate induced by MHD turbulence according to the model of Geertsema & Achterberg (1992), we find that the quiescent disc viscosity parameter in V4140 Sgr is large ($\alpha \simeq 0.2-0.4$) at all disc radii, in agreement with MTIM predictions and in marked contrast with DIM predictions. The discrepancy between the inferred α values and DIM predictions is statistically significant at the 2σ confidence level outside the region $0.2 \leq R/R_{L1} \leq 0.3$.

The high-viscosity, steady-state quiescent disc of V4140 Sgr and the inferred low disc temperatures in superoutburst are inconsistent with expectations of the disc-instability model, and lead to the conclusion that the outbursts of V4140 Sgr are powered by the only other mech-

anism considered so far, namely, bursts of enhanced mass transfer rate from its donor star.

The dominant source of uncertainty in the computed $\alpha(R)$ distribution are the errors in the relative amplitude of the high-frequency, disc-related flickering component. These errors can be reduced by increasing the S/N of the flickering curves, i.e., by increasing the statistics and/or the S/N of the individual light curves included in the data sample. The benefits of this observational effort are double: it will allow a more meaningful and statistically robust estimate of the magnitude of the disc viscosity parameter and it will open the possibility to properly probe changes in α with radius.

6 ACKNOWLEDGEMENTS

We thank an anonymous referee for useful comments and suggestions which helped to improve the presentation of our results. RB acknowledges financial support from CNPq/Brazil through grant 308 946/2011-1. ASO acknowledges FAPESP for financial support under grant 03/12618-7.

APPENDIX A: PERFORMANCE TESTS OF THE 3D ECLIPSE MAPPING

Here we report simulations aimed to show the performance of our 3D eclipse mapping code in reproducing accretion disc brightness distributions with out-of-eclipse modulations. We also show how the entropy of the eclipse map can be used to constrain the disc half-opening angle β and the disc rim radius R_d .

We illustrate the performance of the 3D eclipse mapping code with reconstructions from a synthetic eclipse map comprised of a steady-state ($T \propto R^{-3/4}$), axi-symmetric disc brightness distribution plus a bright spot “painted” in the disc rim at an azimuth of $\theta_{bs} = +30^\circ$ (azimuths are counted counter-clockwise from the line joining both stars). This model distribution is shown in Fig. A1(a). It was convolved with the eclipse geometry of V4140 Sgr ($i = 80.2^\circ, q = 0.125$) and pairs of values (β, R_d) to generate synthetic light curves to which gaussian noise was added in order to simulate real data. Each of these light curves were then subjected to the 3D eclipse mapping code.

If an eclipse mapping reconstruction is performed with the wrong choice of β and R_d , the code will develop artifacts in the brightness distribution in order to compensate for the incorrect parameters. This is illustrated in Fig. A1. A synthetic light curve with added Gaussian noise ($S/N = 50$) was generated from the brightness distribution of Fig. A1(a) and reconstructions were obtained for different combinations of β and R_d . Fig. A1(b) shows a reconstruction with the correct geometry $\beta = 2.0^\circ, R_d = 0.5 R_{L1}$. The disc surface brightness distribution and the azimuth of the spot at disc rim are well recovered. The azimuthal blur of the spot at disc rim is intrinsic to the eclipse mapping method and is controlled by the choice of $\Delta\theta$ (see Sect. 3.3). Figs. A1(c) and (d) show the effects of errors in the choice of β . Underestimating (overestimating) the disc half-opening angle forces the code to artificially increase the brightness of the disc hemisphere farther away from (closest to) the L1 point to compensate for their lower effective area during eclipse. Eclipse maps with these

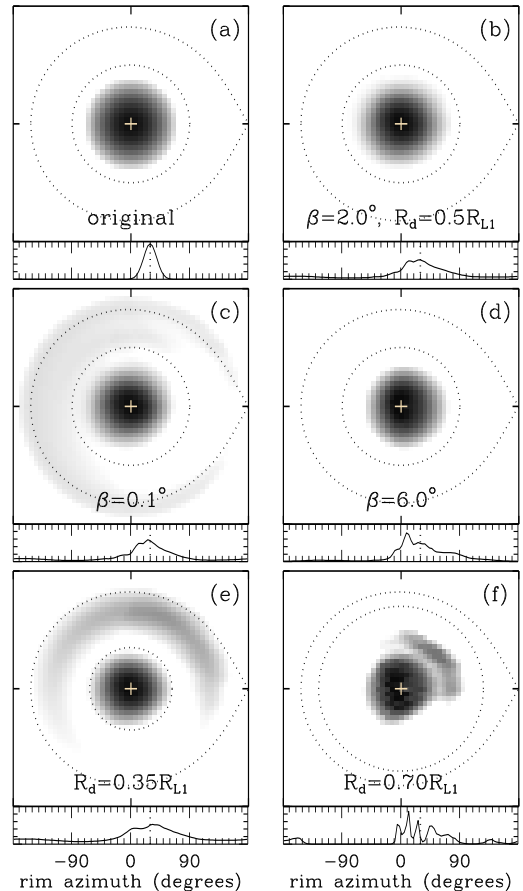


Figure A1. (a): Logarithmic grayscale representation of the synthetic brightness distribution used in the simulations (dark regions are brighter). A cross marks the disc centre and dotted lines depict the primary Roche lobe and the circular disc rim at radius R_d . The lower inset shows the intensity distribution along the disc rim. Azimuths are counted from the line joining both stars and increase counter-clockwise. (b) A reconstruction using the correct geometry, $\beta = 2.0^\circ, R_d = 0.5 R_{L1}$. (c) A reconstruction with correct R_d but underestimated $\beta = 0.1^\circ$. (d) The same as in (c) for an overestimated $\beta = 6.0^\circ$. (e) A reconstruction with correct β but underestimated $R_d = 0.35 R_{L1}$. (f) The same as in (e) for an overestimated $R_d = 0.70 R_{L1}$.

spurious, additional structures have lower entropy than the map with the correct choice of β and R_d ⁶. Figs. A1(e) and (f) show the effects of errors in the choice of R_d . Again, artifacts develop in the disc brightness distribution in order to compensate for the wrong radial position of the disc rim. In both cases, the additional asymmetry leads to eclipse maps of lower entropy. Because of these artifacts, reconstructions obtained with a wrong choice of (β, R_d) have lower entropy than that with the correct combination of parameters.

Therefore, it is possible to use the entropy of the eclipse

⁶ The entropy S measures the amount of structure in an eclipse map. The more structured an eclipse map is, the lower its entropy is. The map of highest entropy S_{\max} is the one with the least amount of structures allowed by the data.

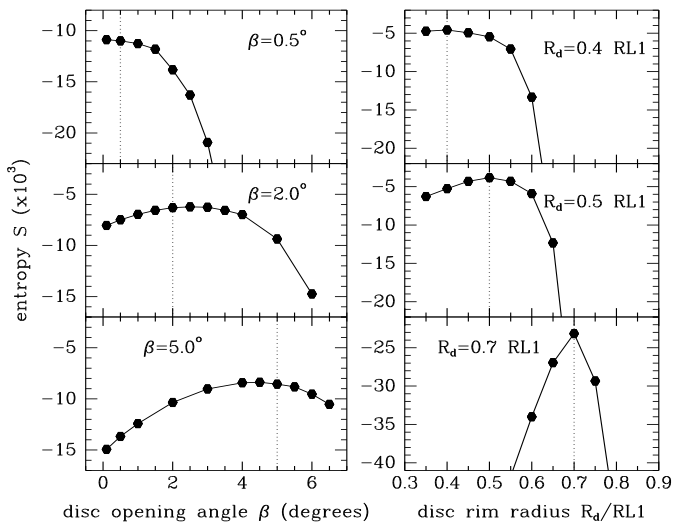


Figure A2. The entropy of the eclipse map as a function of β (left-hand panels) and R_d (right-hand panels). In each panel, the correct value of β or R_d is labeled and depicted as a vertical dotted line.

map as a tool to gauge the correct choice of (β, R_d) . In order to do this, we obtain reconstructions covering the space of parameters (β, R_d) with a suitable sampling and we search for the combination which leads to the reconstruction of highest entropy $(\beta(S_{\max}), R_d(S_{\max}))$. This is called ‘entropy landscape’, a technique that has been successfully used to find best-fit parameters with other image reconstruction methods (e.g., [Rutten & Dhillon 1994](#)). Fig. A2 illustrates the procedure. We generated an input synthetic light curve ($S/N = 50$) from the brightness distribution of Fig. A1(a) for a given combination of parameters (β_i, R_{d_i}) and obtained reconstructions of that light curve for a range of (β, R_d) values. The space of parameters is covered by sampling β in the range $(0^\circ - 6^\circ)$ at steps of 0.5° , and by sampling R_d in the range $(0.35 - 0.85) R_{L1}$ at steps of $0.05 R_{L1}$. The left-hand panels show the entropy of the reconstruction as a function of β for light curves obtained with three different β_i values and fixed $R_d = R_{d_i}$, whereas the right-hand panels show the entropy of the reconstruction as a function of R_d for light curves obtained with three different R_{d_i} values and fixed $\beta = \beta_i$. It is possible to recover the correct value of β with an accuracy of $\pm 0.5^\circ$, and the correct value of R_d with an accuracy of $\pm 0.05 R_{L1}$. These results are confirmed with a series of simulations with several different brightness distributions and light curves with S/N comparable to those of the V4140 Sgr data.

REFERENCES

Balbus, S.A., & Hawley, J.F. 1991. *ApJ*, 376, 214
 Balbus, S.A., & Hawley, J.F. 1998. *RvMP*, 70, 1
 Baptista, R. 2001. in *Astromotography, Indirect Imaging Methods in Observational Astronomy*, Lecture Notes in Physics 573, ed. H. M. J. Boffin, D. Steeghs, & J. Cuypers (Berlin: Springer), 307
 Baptista, R. 2012. *Mem. Soc. Astr. It.*, 75, 282
 Baptista, R., & Bortoletto, A. 2004. *AJ*, 128, 411

Baptista, R., & Bortoletto, A. 2008. *ApJ*, 676, 1240
 Baptista, R., & Catalán, M. S. 2001. *MNRAS*, 324, 599
 Baptista, R., Horne, K., Wade, R., Hubeny, I., Long, K. S., & Rutten, R. G. M. 1998. *MNRAS*, 298, 1079
 Baptista, R., Jablonski, F. J., & Steiner, J. E. 1989. *MNRAS*, 241, 631
 Baptista, R., Morales-Rueda, L., Harlaftis, E. T., Marsh, T. R., & Steeghs, D. 2005. *A&A*, 444, 201
 Baptista, R., Santos, R. F., Faúndez-Abans, M., & Bortoletto, A. 2007. *AJ*, 134, 867
 Baptista, R., & Steiner, J. E. 1993. *A&A*, 277, 331
 Baptista, R., Steiner, J. E., Horne, K. 1996. *MNRAS*, 282, 99
 Bath, G. T. 1975. *MNRAS*, 171, 311
 Beckwith, K., Armitage, P. J., & Simon, J. B. 2011. *MNRAS*, 416, 361
 Bennie, P. J., Hilditch, R., & Horne, K. 1996. in *IAU Colloq. 158, Cataclysmic Variables and Related Objects*, ed. A. Evans & J. H. Wood (Dordrecht: Kluwer), 33
 Bessell, M. A. 1990. *PASP*, 102, 1181
 Borges, B., Baptista, R. 2005. *A&A*, 437, 235
 Bobinger, A., Horne, K., Mantel, K.-H., Wolf, S. 1997. *A&A*, 327, 1023
 Bruch, A. 1992. *A&A*, 266, 237
 Bruch, A. 1996. *A&A*, 312, 97
 Bruch, A. 2000. *A&A*, 359, 998
 Bruch, A., Beele, D., Baptista, R. 1996. *A&A*, 306, 151
 Cannizzo, J. K. 1993. *ApJ*, 419, 318
 Efron, B., 1982. *The Jackknife, The Bootstrap and Other Resampling Plans* (SIAM, Philadelphia 1982)
 Eggleton, P. P., 1983. *ApJ*, 268, 368
 Elsworth, Y. P. & James, J. F. 1982. *MNRAS*, 198, 889
 Frank, J., King, A., & Raine D. 2002. *Accretion Power in Astrophysics - 3rd. edition*, (Cambridge: Cambridge Univ. Press)
 Graham, J. A. 1982. *PASP*, 94, 244
 Geertsema, G. T. & Achterberg, A. 1992. *A&A*, 255, 427
 Hameury J.-M., & Lasota, J.-P. 2014. *A&A*, 569, A48
 Hawley, J.F., & Balbus, S.A. 1991. *ApJ*, 376, 223
 Hellier, C., et al. 2000. *MNRAS*, 313, 703
 Hellier, C. 2001. *Cataclysmic Variable Stars: How and why they vary* (Chichester: Springer-Praxis)
 Hessman, F. V., & Hopp, U. 1990. *A&A*, 228, 387
 Hirose, M., & Osaki, Y. 1990. *PASJ*, 42, 135
 Hirose, M., Osaki, Y., & Mineshige, S. 1991. *PASJ*, 43, 809
 Hirose, S., Blaes, O., Krolik, J. H., Coleman, M. S. B., & Sano, T. 2014. *ApJ*, 787, 1
 Hoaglin, D. C., Mosteller, F., & Tukey, J. W. 1983. *Understanding Robust and Exploratory Data Analysis* (New York: John Wiley & Sons)
 Horne, K. 1985. *MNRAS*, 213, 129
 Horne, K., Cook, M. C. 1985. *MNRAS*, 214, 307
 Horne, K., & Stiening, R. F. 1985. *MNRAS*, 216, 933
 Jablonski, F. & Steiner, J. E. 1987. *ApJ*, 313, 376
 King, A. R., Pringle, J. E., & Livio, M. 2007. *MNRAS*, 376, 1740
 Kawaguchi, T., Mineshige, S., Machida, M., Matsumoto, R. & Shibata K. 2000. *PASJ*, 52, L1
 Lamla, E. 1981. in *Landolt-Börnstein - Numerical Data and Functional Relationships in Science and Technology*, Vol. 2, eds. K. Schaifers & H. H. Voigt (Berlin: Springer-Verlag)
 Lasota, J. P. 2001. *New Astronomy Review*, 45, 449
 Lubow, S. H. 1991. *ApJ*, 381, 259
 Lubow, S. H. 1994. *ApJ*, 432, 224
 Lucke, P. B. 1978. *A&A*, 64, 367
 Marsh, T. R. 1988. *MNRAS*, 231, 1117
 O’Donoghue, D. 1990. *MNRAS*, 246, 29
 Patterson, J., et al. 2000. *PASP*, 112, 1567
 Patterson, J., et al. 2005. *PASP*, 117, 1204
 Press, W. H., Flannery, B. P., Teukolsky, S. A., & Vetterling,

- W. T. 1992. Numerical Recipes in C (Cambridge: Cambridge University Press)
- Ribeiro, T., Baptista, R., Harlaftis, E. T., Dhillon, V. S. & Rutten, R. G. M. 2007. *A&A*, 474, 213
- Rolfe, D., Haswell, C. A., Patterson, J. 2000. *MNRAS*, 317, 759
- Rutten, R. G. M. 1998. *A&AS*, 127, 581
- Rutten, R. G. M., & Dhillon, V. K. 1994. *A&A*, 288, 773
- Rutten, R. G. M., van Paradijs, J. & Tinbergen, J. 1992. *A&A*, 260, 213
- Shakura, N. I. & Sunyaev, R. A. 1973. *A&A*, 24, 337
- Shu, F. H. 1976. in *Structure and Evolution of Close Binary Systems*, ed. P. Eggleton, S. Mitton & J. Whelan, Dordrecht, 253
- Smak, J. 1971. *Acta Astron.*, 21, 15
- Stone, R. P. S., & Baldwin, J. A. 1983. *MNRAS*, 204, 347
- Sulkanen, M. E., Brasuke, L. W. & Patterson, J. 1981. *ApJ*, 244, 579
- Truss, M. R., Wynn, G. A., & Wheatley, P. J. 2004. *MNRAS*, 347, 569
- Warner, B. 1995. *Cataclysmic Variable Stars* (Cambridge: Cambridge University Press)
- Warner, B. & Nather, R. E. 1971. *MNRAS*, 152, 219
- Watson, C. A., & Dhillon, V. S. 2001. *MNRAS*, 326, 67
- Whitehurst, R. 1988. *MNRAS*, 232, 35
- Whitehurst, R., & King, A. 1991. *MNRAS*, 249, 25
- Wood, J. H., et al. 1989. *MNRAS*, 239, 809

This paper has been typeset from a $\text{\TeX}/\text{\LaTeX}$ file prepared by the author.